Ultrafast Science
A SCIENCE PARTNER JOURNAL

RESEARCH ARTICLE

Identification of the Decay Pathway of Photoexcited Nucleobases

Xiangxu Mu[1†], Ming Zhang[1†], Jiechao Feng[1], Hanwei Yang[1], Nikita Medvedev[2], Xinyang Liu[1], Leyi Yang[1], Zhenxiang Wu[1], Haitan Xu[3,4,5*], and Zheng Li[1,6,7*]

[1]State Key Laboratory for Mesoscopic Physics and Collaborative Innovation Center of Quantum Matter, School of Physics, Peking University, Beijing 100871, China. [2]Institute of Physics Czech Academy of Science, Na Slovance 2, 182 21 Prague 8, Czech Republic. [3]School of Materials Science and Intelligent Engineering, Nanjing University, Suzhou 215163, China. [4]Shenzhen Institute for Quantum Science and Engineering, Southern University of Science and Technology, Shenzhen, China. [5]School of Physical Sciences, University of Science and Technology of China, Hefei 230026, China. [6]Collaborative Innovation Center of Extreme Optics, Shanxi University, Taiyuan, Shanxi 030006, China. [7]Peking University Yangtze Delta Institute of Optoelectronics, Nantong, Jiangsu 226010, China.

*Address correspondence to: haitanxu@nju.edu.cn (H.X.); zheng.li@pku.edu.cn (Z.L.)
†These authors contributed equally to this work.

Citation: Mu X, Zhang M, Feng J, Yang H, Medvedev N, Liu X, Yang L, Wu Z, Xu H, Li Z. Identification of the Decay Pathway of Photoexcited Nucleobases. *Ultrafast Sci.* 2023;3:Article 0015. https://doi.org/10.34133/ultrafastscience.0015

Submitted 13 September 2022
Accepted 23 December 2022
Published 8 March 2023

The identification of the decay pathway of the nucleobase uracil after being photoexcited by ultraviolet light has been a long-standing problem. Various theoretical models have been proposed but yet to be verified. Here, we propose an experimental scheme to test the theoretical models of gas phase uracil decay mechanism by a combination of ultrafast x-ray spectroscopy, x-ray diffraction, and electron diffraction methods. Incorporating the signatures of multiple probing methods, we demonstrate an approach that can identify the dominant mechanism of the geometric and electronic relaxation of the photoexcited uracil molecule among several candidate models.

Introduction

Ultraviolet photons in the sunlight can excite biological molecules, and the photoexcited molecules then experience different interatomic potential energies, which may induce unexpected reactions, such as dimethylation of RNA and DNA molecules, and seriously harm the biological functions of the molecules [1,2]. In order to survive from the photodamage, living things seem to have chosen a special set of molecules as building blocks, which can decay rapidly at an ultrafast time scale via nonadiabatic pathways before harmful reactions take place [3,4]. However, surprisingly, it was proposed that uracil, one of the nucleobases, could have a different property when being photoexcited to the singlet state S_2 by ultraviolet light. Theoretical investigations showed that a single uracil molecule in the gas phase may have a substantially longer electronic decay time up to picoseconds (ps) from the photoexcited state because of a hypothetical barrier blocking the pathway to the conical intersection (CI) between the S_2/S_1 states (see Fig. 1A) [5]. CI is a diabolical point in the potential energy surface caused by pointwise degeneracy of different electronic states and provides an ultrafast route of nonadiabatic electronic decay [6–9]. The instability of RNA due to the long decay time of photoexcited uracil may result in gene mutations and evolution of life. On the other hand, the proposal of ps-long decay time of uracil is challenged by the follow-up studies [10–17], because the predicted potential barrier of ~0.2 eV is very shallow, and because of the precision limit of quantum chemical calculations, different methods give contradictory predictions of electronic decay pathways.

The controversial predictions cover various time scales of electronic decay from the photoexcited S_2 state (see Fig. 1B). The long trajectory hypothesis [5] assumes that the relaxation is a 2-step process. After being excited to S_2 from the ground state at the Franck–Condon (FC) region, the uracil first takes ~100 fs to relax to a deformed geometry of minimal energy (ME) in the S_2 state and then reaches the minimal energy conical intersection (MECI) between S_2 and S_1 states for the electronic decay, which could take ps because of the potential energy barrier of about 0.2 eV, as shown in Fig. 1A. The short trajectory hypothesis assumes that the uracil decays to S_1 in about 70 fs, and the nonadiabatic transition follows rapidly for an undistorted geometry [11]. The intermediate trajectory hypothesis points to the third possibility of the decay pathway. The uracil can partially circumvent the barrier and evolve to a CI point between S_2 and S_0 within ~0.7 ps, which is energetically not favored but can result in direct transition to the ground state S_0 [10], and the intermediate state S_1 does not participate in this pathway.

Here, we propose an approach to resolve the debate, which can uniquely identify the electronic decay mechanism of the

photoexcited uracil by means of ultrafast x-ray spectroscopy and coherent diffraction imaging. Without participating in the debate over the correctness of various decay models, we show that the combined ultrafast spectroscopic and diffraction signals are different for different decay models. Therefore, by comparing experimental outcomes with the predicted signals for the various decay models, one can identify the dominant mechanism in reality. The ultrafast electron diffraction (UED) is capable of characterizing the evolving mean distance between electrons [19] and molecular geometry [20] and can be used to monitor the electronic population transfer and transient structural dynamics [21]. The ultrafast x-ray diffraction (UXD), although less sensitive to the mean distance variation between electrons, is free of pulse length limitation of UED because of space charge effect of electron bunch compression. For UXD with attosecond time resolution [22,23], it can resolve the transient geometric structure with higher temporal precision. The x-ray photoelectron spectroscopy (XPS) equipped with the ultrashort x-ray pulses from free electron lasers provides the toolkit to map out the valence electron density variation in the chosen atomic sites of molecules in the excited state. Incorporating the mixed quantum–classical surface hopping molecular dynamics (MD) method [24], we simulate the trajectories that follow the long trajectory hypothesis, using the ab initio 5-state averaged complete active space self-consistent field method with 8 active electrons in 6 orbitals (SA5-CASSCF(8,6)) and 6-31g* basis set [5], in order to show that a joint analysis based on UED, UXD, and XPS data can test this hypothesis. The surface hopping MD simulation of photoexcited uracil and the calculation of spectral and diffraction observables are carried out using the SHARC package [15,25], as well as the quantum chemistry packages Molpro [26] and Terachem [27], respectively (see details of the MD simulation in Supplementary Information [SI]). This joint analysis is self-consistent with our simulation.

Methods

Here, we demonstrate the methods to calculate XPS and UED signals for single-point geometries, which are then used to simulate the time-resolved XPS spectra and patterns from MD trajectories.

First, the x-ray photoelectron spectra of photoexcited uracil at a given geometry can be calculated under dipole approximation; the ionization rate from the initial state $|\psi_I\rangle$ with energy E_I is:

$$P(E) \propto \sum_{f,\eta} \left| \left\langle \psi_f \phi_\eta \left| \hat{\vec{\mu}} \cdot \vec{\mathscr{E}} \right| \psi_I \right\rangle \right|^2 \delta\left(\hbar\omega + E_I - E_f - E\right), \quad (1)$$

where the final state includes the molecular cationic state $|\psi_f\rangle$ with energy E_f and the ejected electron state $|\phi_\eta\rangle$ with energy E, $\hbar\omega$ is the x-ray photon energy, and $\hat{\vec{\mu}}$ and $\vec{\mathscr{E}}$ are the electronic dipole operator and the electric field of x-ray. In the second quantized form,

$$\left\langle \psi_f \phi_\eta \left| \hat{\vec{\mu}} \cdot \vec{\mathscr{E}} \right| \psi_I \right\rangle = \sum_{ij} < \psi_f \phi_\eta \left| \hat{a}_i^\dagger \hat{a}_j \right| \psi_I \rangle \vec{\mu}_{ij} \cdot \vec{\mathscr{E}} = \sum_j < \psi_f \left| \hat{a}_j \right| \psi_I \rangle \vec{\mu}_{\eta j} \cdot \vec{\mathscr{E}}, \quad (2)$$

where i,j are orbital indexes including all bounded and continuum states. $\vec{\mu}_{ij}$ is the matrix element of transition dipole moment between the corresponding initial and final orbitals. Because the $|\phi_\eta\rangle$ orbital in the continuum is not occupied in the initial state $|\psi_I\rangle$, the creation operator index i equals to η for nonzero terms in the summation. Because we only consider the carbon K-edge energy range covered by the chosen XPS probe, the orbital index j of the ionized electron is replaced by

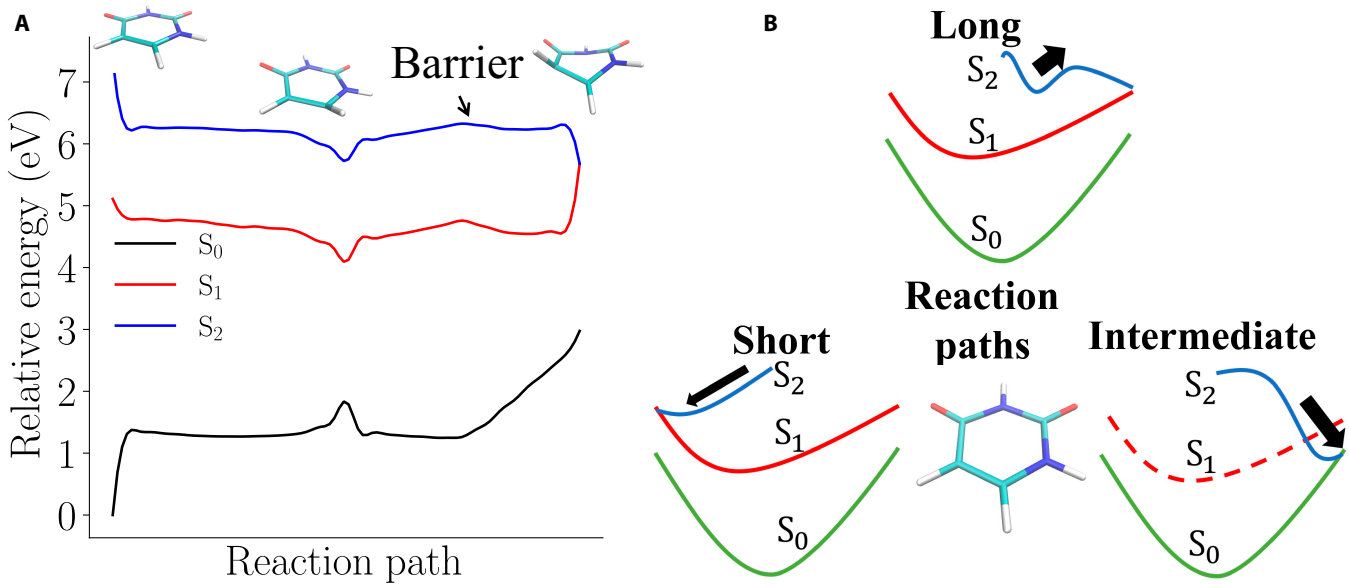

Fig.1. Predicted pathways for the electronic decay of photoexcited uracil in the gas phase. (A) Potential energy curves for the reaction path of the long pathway, including the ME (S_0), ME (S_2), and MECI (S_2/S_1) geometries [5], which are determined by the nudged elastic band method [18], and the geometries are optimized on the SA5-CASSCF(8,6)//6-31g* level. There is a barrier of about 0.2 eV from ME (S_2) to MECI (S_2/S_1). (B) Sketches of the 3 hypotheses of reaction paths and the equilibrium geometry of the uracil in the ground state. The long trajectory hypothesis assumes that the uracil relaxes into minimum energy geometry in the S_2 state within about 100 fs and then reaches the minimal energy conical intersection (MECI) between S_2 and S_1 states in several picoseconds (ps). The short trajectory hypothesis assumes that the uracil arrives at S_1 in about 70 fs [11]. The intermediate trajectory hypothesis assumes that part of the uracil evolves to a CI point between S_2 and S_0 states within about 0.7 ps [10].

p, which is restricted to the set of carbon 1s orbitals. Adopting the approximation $\vec{\mu}_{\eta p} \cdot \vec{\mathcal{E}} \approx f(E)$ from [5], the XPS spectra can be approximately obtained by:

$$P(E) \propto \sum_f \left| \sum_p < \psi_f | \hat{a}_p | \psi_I > \right|^2 \rho(E) f(E) \delta\left(\hbar\omega + E_I - E_f - E\right) \tag{3}$$

where $\rho(E)$ is the density of state. For photoionization in the low-energy region far from resonance, the product $\rho(E)f(E)$ can be treated as a constant [5], so that:

$$P(E) \propto \sum_f \left| \sum_p < \psi_f | \hat{a}_p | \psi_I > \right|^2 \delta\left(\hbar\omega + E_I - E_f - E\right). \tag{4}$$

We use identical molecular orbitals (MOs) for ψ_f and ψ_I optimized by complete active space self-consistent field (CASSCF) method for the initial-state wave function ψ_I, so that $< \psi_f \mid \hat{a}_p \mid \psi_I >$ can be calculated from the corresponding CI coefficients. For final-state wave function ψ_f, the complete active space configuration interaction calculation is performed to optimize the configuration interaction wave function coefficients with the same set of MOs as the initial-state wave function ψ_I. The calculation involves 3 initial states S_0, S_1, and S_2, and for each carbon $1s^{-1}$ hole, 50 cationic final states with lowest energy were included in the calculation.

Second, UED provides a tool for retrieving transient molecular structural and electronic dynamics simultaneously [19] and exhibits high sensitivity to the mean distance between electrons from small-angle scattering signals. The intensities of the elastic and inelastic scattering signals are,

$$I_{\text{elastic}}\left(\vec{s}\right) = \frac{1}{s^4} \left| \sum_\alpha N_\alpha e^{i\vec{s}\cdot\vec{R}_\alpha} - f\left(\vec{s}\right) \right|^2, \tag{5}$$

$$I_{\text{inelastic}}\left(\vec{s}\right) = \frac{1}{s^4} \left[n + P\left(\vec{s}\right) - \left| f\left(\vec{s}\right) \right|^2 \right], \tag{6}$$

where $\vec{s} = \vec{k}_{\text{in}} - \vec{k}_{\text{out}}$ is the momentum transfer of electrons, N_α and $\vec{R}_\alpha$ are the nuclear charge and position of the αth atom, n is the number of electrons in the molecule, and $f\left(\vec{s}\right)$ and $P\left(\vec{s}\right)$ are the Fourier transforms of 1-electron density $\rho\left(\vec{r}\right)$ and 2-electron density $\rho^{(2)}\left(\vec{r},\vec{r}\,'\right)$,

$$f\left(\vec{s}\right) = \int e^{i\vec{s}\cdot\vec{r}} \rho\left(\vec{r}\right) d\vec{r} = \sum_{ij} \gamma_{ij}^{(1)} \int e^{i\vec{s}\cdot\vec{r}} \phi_i^*\left(\vec{r}\right) \phi_j\left(\vec{r}\right) d\vec{r} = \sum_{ij} \gamma_{ij}^{(1)} \Phi_{ij}\left(\vec{s}\right), \tag{7}$$

$$P\left(\vec{s}\right) = \int e^{i\vec{s}\cdot(\vec{r}-\vec{r}\,')} \rho^{(2)}\left(\vec{r},\vec{r}\,'\right) d\vec{r}\, d\vec{r}\,'$$
$$= \sum_{ijkl} \gamma_{ijkl}^{(2)} \int e^{i\vec{s}\cdot(\vec{r}-\vec{r}\,')} \phi_i^*\left(\vec{r}\right) \phi_j\left(\vec{r}\right) \phi_k^*\left(\vec{r}\,'\right) \phi_l\left(\vec{r}\,'\right) d\vec{r}\, d\vec{r}\,' = \sum_{ijkl} \gamma_{ijkl}^{(2)} \Phi_{ij}\left(\vec{s}\right) \Phi_{kl}\left(-\vec{s}\right) \tag{8}$$

Here, $\phi_i\left(\vec{r}\right)$ is the ith MO, $\gamma_{ij}^{(1)}$ and $\gamma_{ijkl}^{(2)}$ are matrix elements of 1-electron and 2-electron reduced density matrix (1RDM and 2RDM), and $\Phi_{ij}\left(\vec{s}\right) = \int e^{i\vec{s}\cdot\vec{r}} \phi_i^*\left(\vec{r}\right) \phi_j\left(\vec{r}\right) d\vec{r}$ is the Fourier integrals of MO basis functions.

The 1RDM and 2RDM can be obtained from CASSCF wave function. The matrix elements for doubly occupied closed orbitals i,j,k,l are:

$$\gamma_{ij}^{(1)} = 2\delta_{ij}, \tag{9}$$

$$\gamma_{ijkl}^{(2)} = 4\delta_{ij}\delta_{kl} - 2\delta_{jk}\delta_{il}. \tag{10}$$

The 2RDM elements between closed orbitals i,j and active orbitals t,u are:

$$\gamma_{ijtu}^{(2)} = \gamma_{tuij}^{(2)} = 2\delta_{ij}\gamma_{tu}^{(1)}, \tag{11}$$

$$\gamma_{ituj}^{(2)} = \gamma_{tiju}^{(2)} = -\delta_{ij}\gamma_{tu}^{(1)}. \tag{12}$$

So the diffraction integrals $f\left(\vec{s}\right)$ and $P\left(\vec{s}\right)$ can be expressed as:

$$f\left(\vec{s}\right) = 2 \sum_j^{\text{closed}} \Phi_{jj}\left(\vec{s}\right) + \sum_{tu}^{\text{active}} \gamma_{tu}^{(1)} \Phi_{tu}\left(\vec{s}\right), \tag{13}$$

$$P\left(\vec{s}\right) = \left| 2 \sum_j^{\text{closed}} \Phi_{jj}\left(\vec{s}\right) \right|^2 - 2 \sum_{ij}^{\text{closed}} \left| \Phi_{ij}\left(\vec{s}\right) \right|^2 + \sum_{tuvw}^{\text{active}} \gamma_{tuvw}^{(2)} \Phi_{tu}\left(\vec{s}\right) \Phi_{wv}^*\left(\vec{s}\right)$$
$$+ 2 \sum_i^{\text{closed}} \sum_{tu}^{\text{active}} \gamma_{tu}^{(1)} \left[\Phi_{tu}\left(\vec{s}\right) \Phi_{ii}^*\left(\vec{s}\right) + \Phi_{ii}\left(\vec{s}\right) \Phi_{ut}^*\left(\vec{s}\right) \right] - 2 \sum_i^{\text{closed}} \sum_{tu}^{\text{active}} \gamma_{tu}^{(1)} \Phi_{ti}\left(\vec{s}\right) \Phi_{ui}^*\left(\vec{s}\right) \tag{14}$$

The elastic and inelastic diffraction intensity can be calculated by Eqs. 5 and 6.

The inelastic scattering intensity $I_{\text{inelastic}}\left(\vec{s}\right)$ dominates at small scattering angles. Because the inelastic electron scattering is dependent on the Fourier transform of the 2-electron density $\rho^{(2)}\left(\vec{r},\vec{r}\,'\right)$, it measures the changes in the mean distance between electrons due to the transitions of electronic states [19]. In contrast, the elastic scattering signal $I_{\text{elastic}}\left(\vec{s}\right)$ dominates at larger scattering angles and encodes the transient structural information characterized by the atomic charge pair distribution functions (CPDF) [21,28], which are given by:

$$\text{CPDF}(R,t) = R \int_0^{s_{\max}} s^5 I(s,t) e^{-\alpha s^2} \sin(sR) ds, \tag{15}$$

where $I(s,t)$ is the isotropic average of the total UED signal including both elastic and inelastic components. The damping term $e^{-\alpha s^2}$ with $\alpha = 0.06$ is introduced to avoid edge effects during the transform [28].

Results and Discussion

XPS can help to distinguish electronic state of molecule by analyzing the local charge distribution around the specific atoms.

Choosing the carbon K-edge for the x-ray probe, the shift of photoelectron energy of XPS in the molecule compared to that of carbon atom reflects the strength of electron screening of nuclear charge [29] and maps out the local density of valence electrons at the specific atom, from which the 1s core electron is ionized, as shown in Fig. 2A. Because the excitation to the S_1 and S_2 states is accompanied by the flow of valence electrons from the nonbonding (n) and bonding π orbitals to the antibonding π^* orbital of uracil, the deficit and excess of valence

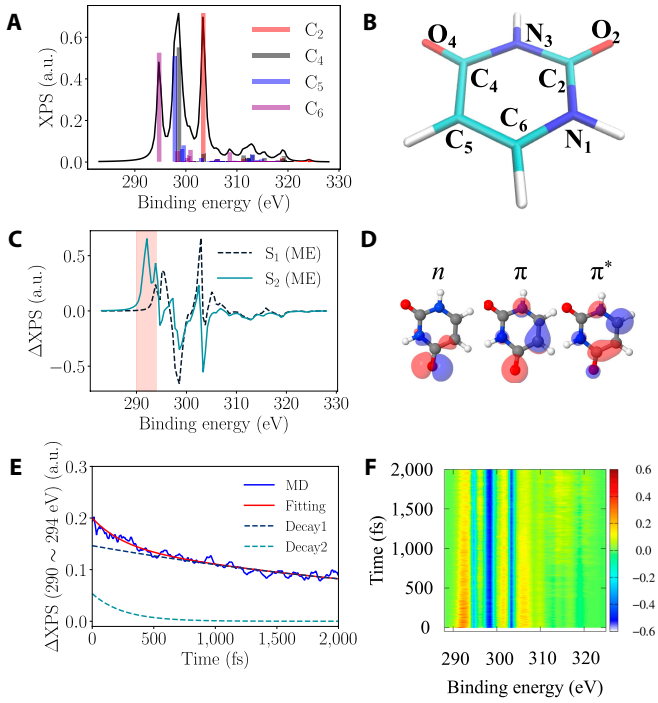

Fig. 2. Calculated XPS signals and their variations (ΔXPS) with respect to the electronic state transitions of uracil. (A) XPS of ground state. The colored columns mark the intensity of transition to ionized final states, where the $1s^{-1}$ hole is located at 1 of the 4 individual carbon atoms with different K-shell binding energies. (B) Geometry with minimum energy. (C) ΔXPS of minimum energy geometry of S_1 (dashed line) and S_2 (cyan line) states relative to that of ground state S_0. (D) Molecular orbitals that are mostly relevant to the excited S_1 and S_2 states with $n\pi^*$ and $\pi\pi^*$ characters. (E) Temporal evolution of ΔXPS intensity integrated over the energy range from 290 to 294 eV with MD simulation (blue curve) and biexponential fitting (red curve). The 2 components of the biexponential fitting are also plotted, with decay time constants of 249 fs (black dashed curve) and 3,469 fs (cyan dashed curve). (f) Energy-resolved temporal evolution of ΔXPS intensity with MD simulation, the MD is initiated in the excited electronic state S_2, and the photoexcited uracil then relaxes to lower electronic states. a.u., arbitrary units.

electron density on the 4 individual carbon atoms gives the blue- and redshift of carbon 1s binding energies in the XPS spectra, respectively (see Fig. 2B). In the SI, we present the XPS spectra of uracil in the states involved in the MD simulation, including the singlet and triplet excited states. The Mulliken charge analysis of several representative geometries in the long trajectory hypothesis of electronic decay dynamics is shown in Table. The most evident change is the increase of electronic density on C_5 atom in the S_2 state, which leads to the redshift of carbon 1s binding energy followed by the positive peak at 290 eV and the negative peak at 300 eV of ΔXPS of S_2, as shown in Fig. 2C. The change of ΔXPS intensity around 290 eV (shown as the shaded area of Fig. 2C) can be uniquely linked to the evolution population of excited state S_2, because the contribution of S_1 in this spectral range is negligible.

However, apart from the transition of electronic states, the change of molecular geometry can also affect the spectral shift and intensity of ΔXPS, which mixes with the effect from the transition of electronic states and thus prohibits an unambiguous mapping of time-dependent XPS signals to the electronic population evolution (see simulated XPS of different states and geometries in the SI). To quantitatively extract the characteristic time constants of the electronic decay out of the S_2 ($\pi\pi^*$)

Table. The Mulliken charge of 4 individual carbons atoms of Franck–Condon (FC) geometry in the S_0 and S_2 states and minimal energy (ME) geometries in the S_1 and S_2 states; the local charge deficit and excess upon geometric and electronic state variation lead to the blue- and redshift of corresponding binding energies in XPS spectra, respectively.

Structure atom	C_2	C_4	C_5	C_6
FC (S_0)	+1.05	+0.81	−0.32	+0.17
FC (S_2)	+1.05	+0.75	−0.53	+0.13
ME (S_1)	+1.08	+0.69	−0.33	+0.05
ME (S_2)	+1.04	+0.77	−0.46	+0.12

state and nuclear relaxation in the decay of photoexcited uracil, we apply biexponential fitting on ΔXPS(t) [15,30],

$$\Delta\mathrm{XPS}(t) = A_{\mathrm{XPS}}\left[Ne^{-\frac{t}{\tau_1}} + (1-N)e^{-\frac{t}{\tau_2}}\right], \qquad (16)$$

where A_{XPS} is the initial intensity of the ΔXPS(t) signal, and N quantifies the relative components of the geometric and electronic relaxation processes (see details of the fitting procedure in SI). However, the 2 time constants $\tau^1(\mathrm{XPS}) = 249$ fs and $\tau_2(\mathrm{XPS}) = 3468$ fs cannot be unambiguously assigned to the characteristic time scale of geometric relaxation T_α and electronic decay T_β, as the fitting model makes no assumptions about the physics of the temporal trajectory but only quantifies the time scales of the reactions [31]. As the signatures of the 2 relaxation processes mix in the same spectral region, the long and short time constants are not necessarily mapped to the electronic and geometric relaxation time, respectively. In order to resolve this difficulty, we propose a multisignal analysis using spectroscopic (XPS) and diffraction (UED and UXD) signals to investigate these 2 processes and validate the 2 time constants, which can be uniquely assigned to the different types of relaxation processes.

The inelastic scattering intensity $I_{\mathrm{inelastic}}(\vec{s})$ in Eq. 6 dominates at small scattering angles as shown in the shaded area of Fig. 3A.

We define the percentage difference (PD) of the UED signal as

$$\mathrm{PD} = \frac{I_{\mathrm{UED}} - I_{0,\mathrm{UED}}}{I_{0,\mathrm{UED}}} \times 100\,\%, \qquad (17)$$

where $I_{0,\mathrm{UED}}$ is the UED signal in the equilibrium geometry of the ground state and I_{UED} is that of excited states. The S_1 state mainly consists of the characteristic excitation of the localized nonbonding n orbital to delocalized antibonding π^* orbital relative to the ground state S_0 (see Fig. 3B), which is accompanied by the enlarged 2-electron distance and thus the reduction of electronic Coulomb repulsion, which is qualitatively relevant to 2-electron density $\rho^{(2)}(\vec{r},\vec{r}\,')$. Such processes that electrons become further away to each other must result in the enhancement of inelastic scattering signals in momentum space at small scattering angles. The excitation to the S_2 state accompanied by

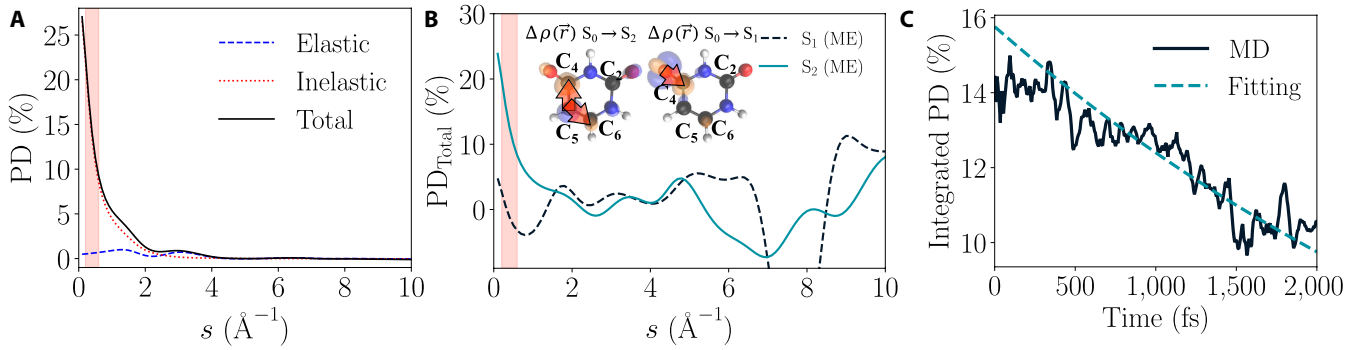

Fig. 3. Simulated UED signal for uracil. (A) Percentage difference (PD) of the UED signals of uracil at the Franck–Condon geometry in the S_2 state. Compared to elastic signal (blue dashed line), inelastic signal (red dotted line) contributes predominantly to the total signal (black line) in the small-angle region. (B) PDs of the total signals for S_1 and S_2 states of the minimum energy structures. Shaded areas in (A) and (B) correspond to the small-angle scattering region $0.2 < s < 0.6 Å^{-1}$. Inset of (B) sketches the variation of electron density $\rho(\vec{r})$ upon transition from S_0 to $n\pi^*$ (S_1) and $\pi\pi^*$ (S_2) states. The orange and blue colors correspond to the positive and negative isosurface $\Delta\rho(\vec{r})$ of $0.01 Å^{-3}$. (C) Temporal evolution of small-angle $PD_{Total}(t)$ of the total signal with the same trajectories surface simulation. The decay time constant is approximately fitted to be τ(UED) ~ 4 ps from the exponential fitting of $PD_{Total}(t)$.

the transition between 2 delocalized orbitals π and π^* leads to longer-range electron flow around the molecular ring. As shown in Fig. 3B, the electrons relocate from the C_5 atom to the 2 nearest neighbor atoms C_4 and C_6, which forms a more delocalized electron density distribution and results in larger PD of inelastic signal than S_1 state in the small s region. Because of the evident PDs of the inelastic scattering signals for S_2 (~20%) and S_1 (<10%) at small angles ($0.2 < s < 0.6$ Å^{-1}) (see Fig. 3B) and for other relevant states (see SI), the inelastic signal can serve as a sensitive probe for the transition of electronic states. We show the PD of the inelastic signal calculated from MD trajectories in Fig. 3C and fit PD(t) with an exponential function as $PD(t) = Ae^{-\frac{t}{\tau}}$. The time constant extracted from the fitting is $\tau(UED) = 4166$ fs, which qualitatively matches the magnitude of electronic decay time constant by time-resolved XPS analysis τ_2(XPS) and correctly reflects the corresponding parameter of the long trajectory model.

Only the temporal inelastic signal at small angle is not sufficient to prove that the uracil transition from S_2 state to S_1 state takes place around the CI geometry. The analysis about geometry information requires the Fourier transformation of the elastic signal, which is called CPDF. However, the fast geometric relaxation [5] could pose a challenge to UED, because its time resolution is partially limited by the space charge effect of the electron pulses. On the other hand, the sub-100-fs structural dynamics can be well resolved by UXD using ultrashort x-ray pulses from x-ray free electron lasers, which can reach an attosecond time resolution [22,23].

To reveal the molecular dynamical information in the simulated UXD data, we apply the spectral and autocorrelation analysis to the CPDF. As shown in Fig. 4B, the black line is the CPDF of uracil at equilibrium FC point. The peak at $R < 1$ Å is contributed by inelastic diffraction, which reflects the mean distance between electrons. The negative CPDF at $R \simeq 1$ Å comes from the electron–nucleus pairs. Longer-range interactions dominate the other peaks, in which the structural information of the atomic positions in the molecule is encoded [28]. The peak at $R \simeq 1.4$ Å comes from the elastic scattering of the nearest neighbor atom pairs, dubbed the first shell. The third peak (at $R \simeq 2.5$ Å) comes from the next nearest neighbor atomic pairs, dubbed the second shell. The fourth peak at $R \simeq$

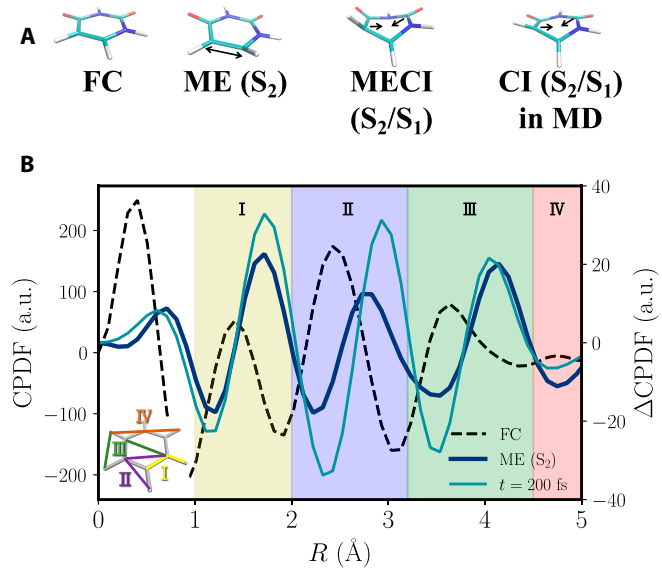

Fig. 4. Charge pair distribution function (CPDF) of static structures and MD trajectories. (A) Geometries of FC, ME (S_2), MECI (S_2/S_1), and a representative CI point. The black arrows depict the major pairwise deformation of the geometries of the equilibrium FC point. (B) CPDF signal of FC (black dashed curve), variation of the CPDF signal of ME (S_2) (blue solid curve), and that of the molecular geometry at the representative time $t = 200$ fs (cyan solid curve). The yellow, purple, green, and red areas correspond to the first shell ($1.0 < R < 2.0$ Å), second shell ($2.0 < R < 3.2$ Å), third shell ($3.2 < R < 4.5$ Å), and fourth shell ($4.5 < R < 5.0$ Å). They are marked by I (yellow), II (purple), III (green), and IV (red), corresponding to those in the inset of (B).

3.8 Å corresponds to the second atomic coordination shell (the distances between atoms are 2 atomic sites; third shell). The fifth peak comes from the third coordination shell (the distances between atoms are 3 atomic sites; fourth shell). The CPDF of charge pairs of various shells are shown in Fig. 4B, marked by I (yellow), II (purple), III (green), and IV (red). The first 3 geometries in Fig. 4A are the same representative configurations as those in Fig. 1A along the reaction path in the S_2 state. A representative CI structure in the MD trajectories is shown in Fig. 4A. The CPDF of other shells are shown in the SI. According to Fig. 4B, as uracil moves toward ME (S_2), the

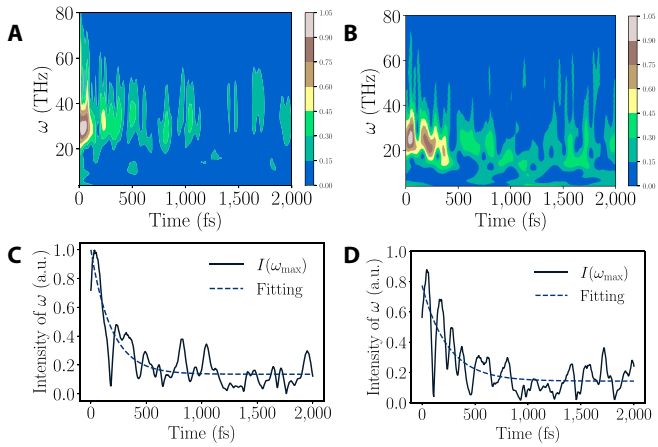

Fig. 5. Dynamics of the geometrical relaxation of the photoexcied uracil. (A) Wavelet transform of autocorrelated bond length evolution of the C_5–C_6 atoms from MD trajectories. (B) Wavelet transform of the detrended autocorrelation function of the CPDF of the ultrafast x-ray diffraction signal $A_{detrend}(t)$ in Eq. 19. (C) Temporal evolution of the vibrational amplitude of the C_5–C_6 bond at $\omega_{max} = 29.2$ THz, with a time constant of 185 fs by exponential fitting. ω_{max} is the frequency where the wavelet transform is maximal when $t = 0$. (D) Temporal evolution of $A_{detrend}$ at $\omega_{max} = 29.2$ THz, with a time constant of 243 fs by exponential fitting.

charge pair density in the first shell increases. These variations of shells manifest themselves clearly in the elastic scattering signal. As shown in the ΔCPDF signal at ME (S_2) in Fig. 4B, compared with the CPDF signal at FC, the peak intensity of the first shell of CPDF moves toward larger R. We also show the ΔCPDF signal at 200 fs from MD trajectories, which is a representative time point near ME (S_2). It exhibits similar positive peak at ~ 2 Å and negative peak at ~ 1 Å and indicates the bond length of C_5–C_6 atoms for ME (S_2) that is the dominant driving reaction coordinate for geometrical relaxation of photoexcited uracil in the long trajectory model [5]. These stretching modes of the C_5 and C_6 atoms are the focus of our quantitative analysis of the structural dynamics. To capture the characteristic signatures of the structural evolution, we apply the continuous wavelet transform analysis to the autocorrelation function of CPDF(t) from the simulated time-resolved UXD signal, which gives the frequency spectra of nuclear motions with largest amplitudes at each time points. The autocorrelation function $A(t)$ is given by:

$$A(t) = \int_{R_a}^{R_b} \mathrm{CPDF}(R,t) \times \mathrm{CPDF}(R,0) dR, \qquad (18)$$

calculated from a swarm of MD trajectories, where R_a and R_b are the boundaries of first atomic shell, and is detrended by a baseline $A_f(t)$ fitted to the exponential model (see details in the SI), giving:

$$A_{\mathrm{detrend}}(t) = A(t) - A_f(t). \qquad (19)$$

In the long trajectory model, the driving mode corresponds to the C_5–C_6 stretching, which is active in the first 500 fs [5]. As shown in the wavelet transformed spectra (Fig. 5A) and the exponential fitting (Fig. 5C) of the evolution of the C_5–C_6 bond length from MD trajectories, the vibrational spectrum peaks around 30 THz at the beginning in the S_2 state for to a period of 33 fs, and this geometric stretching mode dominates around 185 fs. The frequencies of the major modes match that in Fig. 5B, which is obtained from wavelet transform of autocorrelation function of the first shell. Time-dependent frequency spectra of nuclear motion in other shells are shown in the SI. The time constant of the major modes (Fig. 5D), ~243 fs, is also obtained from the exponential fitting of wavelet transform of autocorrelation function of the first-shell CPDF. The analysis shows that the geometric relaxation time scale of <0.5 ps in the long trajectory model can be qualitatively obtained via the time-dependent frequency analysis of ultrafast diffraction with sufficient time resolution.

Conclusion

We have shown that the characteristic time scales of geometric relaxation and electronic decay in the long trajectory model can be faithfully retrieved by incorporating time-resolved XPS, UED, and UXD analysis. In the long trajectory model, the relaxation mechanism of photoexcited uracil is composed of 2 processes. One is the fast geometric relaxation with the characteristic time $T_\alpha < 0.5$ ps, and the other is a slower transition of the electronic state to S_1 with a characteristic time $T_\beta \sim 3$ to 4 ps. It is important to note that none of the 3 methodologies alone can determine the characteristic time constants of the 2 competing relaxation processes of uracil involving nuclear and electronic degrees of freedom.

With the same method, one can test the intermediate and short trajectory hypotheses by experimental measurements. These 2 hypotheses have one major process that is different from the 2-step model in the long trajectory hypothesis. The molecule tends to directly find the decaying geometry in the S_2 state, without first evolving to the minimum energy geometry as in the long trajectory hypothesis. In the short trajectory model (Fig. 1B), the characteristic time of the electronic decay from S_2 to S_1 is less than 100 fs and the molecule keeps the plane geometry, and the CI is very close to the FC region in the S_2 state [11]. In this case, the XPS spectral components of S_2 must decay within 100 fs, which can be observed both in the XPS and the inelastic signal of UED. The CI point in the short trajectory model has a stretched C_5–C_6 bond without the ring-folding characteristic, and the peaks of CPDF are expected to move toward larger R in sub-100 fs, and a similar peak of C_5–C_6 stretching oscillation should appear in the time–frequency analysis of the UXD autocorrelation function. If the molecule decays along the intermediate pathway as shown in Fig. 1B, photoexcited uracil will follow the S_2 state potential energy surface until reaching an ethylenic CI point between S_2 and S_0 [10], which can then decay to the S_0 ground state in ~ 700 fs. In this process, it is expected that the geoemtric relaxation possesses the same time constant as the electronic decay, i.e., ~700 fs, and can be mapped out by XPS and the inelastic part of UED. The UXD offers complementary evidence for the structural dynamics in finding the S_2/S_0 intersection, which should be driven by a small set of reaction coordinates [31]. Such driving coordinates can be revealed by the time–frequency analysis of UXD.

While the predicted phenomena have not yet been fully examined experimentally, they are within reach of the capabilities of free electron lasers and UED facilities. Our study demonstrates the synergy of the XPS and the electron and x-ray diffraction with ultrafast time resolution. The approach can also serve as a general methodological toolkit for investigating valence electron and structural dynamics in ultrafast photochemistry.

Acknowledgments

We thank T. J. Martinez, F. Liu, B. Curchod, J. Yang, and L. Inhester for helpful discussions. **Funding:** This work was supported by the National Natural Science Foundation of China [grant numbers 12174009, 11974031, 12104082, 12234002, and 92250303] and Beijing Natural Science Foundation [grant number Z220008]. N.M. gratefully acknowledges financial support from the Czech Ministry of Education, Youth, and Sports [grant numbers LTT17015, LM2018114, and EF16_013/0001552]. **Author contributions:** Z.L. designed the study. X.M., M.Z., J.F., and H.Y. carried out the calculations. X.M., M.Z., J.F., H.Y., N.M., X.L., L.Y., Z.W., H.X., and Z.L. analyzed the data. All author contributed to the writing of the manuscript. **Competing interests:** The authors declare that there is no conflict of interest regarding the publication of this article.

Data Availability

The data that support the findings of this study are available from the corresponding authors upon reasonable request.

Supplementary Materials

Nonadiabatic tully surface hopping (TSH) molecular dynamics
XPS of uracil in the ground and excited states
Ultrafast electron diffraction
Wavelet transform and time–frequency analysis
Fig. S1. Initial geometries for the molecular dynamics simulation from Wigner distribution.
Fig. S2. Population dynamics for uracil in the first 2 ps of the TSH simulations.
Fig. S3. Characterization of the XPS spectra for various electronic states and molecular geometries.
Fig. S4. Intensity of integrated ΔXPS as a function of time and fitting result of time resolved ΔXPS.
Fig. S5. Ultrafast electron diffraction analysis with comparison between S_2 state at FC point and S_2 state at ME point.
Fig. S6. Time–frequency analysis of various atomic shells.
Table S1. Biexponential fitting result of the integrated ΔXPS.

References

1. Smith DMA, Smets J, Elkadi Y, Adamowicz L. Methylation reduces electron affinity of uracil. Ab Initio theoretical study. *Chem A Eur J*. 1997;101(43):8123.
2. Steenken S, Telo JP, Novais HM, Candeias LP. One-electron-reduction potentials of pyrimidine bases, nucleosides, and nucleotides in aqueous solution. consequences for DNA redox chemistry. *J Am Chem Soc*. 1992;114(12):4701.
3. Wolf TJA, Parrish RM, Myhre RH, Martínez TJ, Koch H, Gühr M. Observation of ultrafast intersystem crossing in thymine by extreme ultraviolet time-resolved photoelectron spectroscopy. *Chem A Eur J*. 2019;123(32):6897–6903.
4. Prokhorenko VI, Picchiotti A, Pola M, Dijkstra AG, Miller RJD. New insights into the photophysics of DNA nucleobases. *J Phys Chem Lett*. 2016;7(22):4445–4450.
5. Hudock HR, Levine BG, Thompson AL, Satzger H, Townsend D, Gador N, Ullrich S, Stolow A, Martínez TJ. Ab initio molecular dynamics and time-resolved photoelectron spectroscopy of electronically excited uracil and thymine. *J Phys Chem A*. 2007;111(34):8500.
6. Yarkony DR. Diabolical conical intersections. *Rev Mod Phys*. 1996;68(4):985–1013.
7. Boggio-Pasqua M, Bearpark MJ, Hunt PA, Robb MA. Dihydroazulene/vinylheptafulvene photochromism: A model for one-way photochemistry via a conical intersection. *J Am Chem Soc*. 2002;124(7):1456.
8. Worth GA, Cederbaum LS. Beyond born-oppenheimer: Molecular dynamics through a conical ntersection. *Annu Rev Phys Chem*. 2004;55(1):127.
9. Domcke W, Yarkony DR. Role of conical intersections in molecular spectroscopy and photoinduced chemical dynamics. *Annu Rev Phys Chem*. 2012;63(1):325.
10. Nachtigallová D, Aquino AJA, Szymczak JJ, Barbatti M, Hobza P, Lischka H. Nonadiabatic dynamics of uracil: Population split among different decay mechanisms. *Chem A Eur J*. 2011;115(21):5247–5255.
11. Lan Z, Fabiano E, Thiel W. Photoinduced nonadiabatic dynamics of pyrimidine nucleobases: On-the-fly surface-hopping study with semiempirical methods. *J Phys Chem B*. 2009;113(11):3548–3555.
12. Chakraborty P, Liu Y, McClung S, Weinacht T, Matsika S. Time resolved photoelectron spectroscopy as a test of electronic structure and nonadiabatic dynamics. *J Phys Chem Lett*. 2021;12(21):5099–5104.
13. Fingerhut BP, Dorfman KE, Mukamel S. Monitoring nonadiabatic dynamics of the RNA base uracil by UV pump–IR probe spectroscopy. *J Phys Chem Lett*. 2013;4(11):1933–1942.
14. Hua W, Mukamel S, Luo Y. Transient X-ray absorption spectral fingerprints of the S_1 dark state in uracil. *J Phys Chem Lett*. 2019;10:7172–7178.
15. Richter M, Mai S, Marquetand P, González L. Ultrafast intersystem crossing dynamics in uracil unravelled by *ab initio* molecular dynamics. *Phys Chem Chem Phys*. 2014;16(44):24423–24436.
16. Brister MM, Crespo-Hernández CE. Direct observation of triplet-state population dynamics in the RNA uracil derivative 1-cyclohexyluracil. *J Phys Chem Lett*. 2015;6(21):4404–4409.
17. Nam Y, Keefer D, Nenov A, Conti I, Aleotti F, Segatta F, Lee JY, Garavelli M, Mukamel S. Conical intersection passages of molecules probed by X-ray diffraction and stimulated raman spectroscopy. *J Phys Chem Lett*. 2021;12(51):12300–12309.
18. Berne BJ, Ciccotti G, Coker DF, *Classical and quantum dynamics in condensed phase simulations*. Singapore: World Scientific; 1998. p. 385.
19. Yang J, Zhu X, F. Nunes JP, Yu JK, Parrish RM, Wolf TJA, Centurion M, Gühr M, Li R, Liu Y, et al. Simultaneous observation of nuclear and electronic dynamics by ultrafast electron diffraction. *Science*. 2020;368:885.
20. Yang J, Zhu X, Wolf TJA, Li Z, Nunes JPF, Coffee R, Cryan JP, Gühr M, Hegazy K, Heinz TF, et al. Imaging CF_3I conical intersection and photodissociation dynamics with ultrafast electron diffraction. *Science*. 2018;361(6397):64–67.
21. Wolf TJA, Sanchez DM, Yang J, Parrish RM, Nunes JPF, Centurion M, Coffee R, Cryan JP, Gühr M, Hegazy K, et al. The photochemical ring-opening of 1,3-cyclohexadiene imaged by ultrafast electron diffraction. *Nat Chem*. 2019;11(6):504–509.
22. Duris J, Li S, Driver T, Champenois EG, MacArthur JP, Lutman AA, Zhang Z, Rosenberger P, Aldrich JW, Coffee R, et al. Tunable isolated attosecond X-ray pulses with gigawatt peak power from a free-electron laser. *Nat Photonics*. 2020;14(1):30–36.
23. Duris JP, MacArthur JP, Glownia JM, Li S, Vetter S, Miahnahri A, Coffee R, Hering P, Fry A, Welch ME, et al. Controllable

x-ray pulse trains from enhanced self-amplified spontaneous emission. *Phys Rev Lett*. 2021;126(10):104802.
24. Tully JC. Molecular dynamics with electronic transitions. *J Chem Phys*. 1990;93(2):1061–1071.
25. Richter M, Marquetand P, González-Vázquez J, Sola I, González L. SHARC: *Ab initio* molecular dynamics with surface hopping in the adiabatic representation including arbitrary couplings. *J Chem Theory Comput*. 2011;7(5):1253–1258.
26. Werner HJ, Knowles PJ, Knizia G, Lindh R, Manby FR, Schütz M, Celani P, Györffy W, Kats D, Korona T, et al. Molpro, version 2012.1, a package of ab initio programs (2012). https://www.molpro.net.
27. Martinez TJ, Ufimtsev IS. Terachem, a package of GPU accelerated ab initio quantum chemistry programs.
28. Yang J, Nunes JPF, Ledbetter K, Biasin E, Centurion M, Chen Z, Cordones AA, Crissman C, Deponte DP, Glenzer SH, et al. Structure retrieval in liquid-phase electron scattering. *Phys Chem Chem Phys*. 2021;23(2):1308–1316.
29. Siegbahn K, Nordling C, Fahlman A, Nordberg R, Hamrin K, Hedman J, Johansson G, Bergmark T, Karlsson S-E; Lindgren, Ingvar and Lindberg. *ESCA: Atomic, molecular and solid state structure studied by means of electron spectroscopy*. Uppsala (Sweden): Almqvist & Wiksells; 1967.
30. McFarland BK, Farrell JP, Miyabe S, Tarantelli F, Aguilar A, Berrah N, Bostedt C, Bozek JD, Bucksbaum PH, Castagna JC, et al. Ultrafast X-ray Auger probing of photoexcited molecular dynamics. *Nat Commun*. 2014;5(1):4235.
31. Gao M, Lu C, Jean-Ruel H, Liu LC, Marx A, Onda K, Koshihara S-y, Nakano Y, Shao X, Hiramatsu T, et al. Mapping molecular motions leading to charge delocalization with ultrabright electrons. *Nature*. 2013;496:343–346.